INVESTIGATION OF ENDWALL FLOWS AND LOSSES IN AXIAL TURBINES. PART I. FORMATION OF ENDWALL FLOWS AND LOSSES

Piotr Lampart

The Szewalski Institute of Fluid-Flow Machinery, Polisch Academy of Science, Gdańsk, Poland
e-mail:lampart@imp.gda.pl

Endwall flows are among the most important sources of loss in turbines. The process of formation of endwall flows and evolution of vorticity from the endwall boundary layers is briefly described in the paper. The resulting endwall losses are discussed. The endwall boundary layer losses are evaluated theoretically by integrating the entropy increase in the boundary layer and assuming a certain model of blade profile load. The endwall losses are also calculated with the help of CFD in a 3D straight turbine cascade of Durham and compared with the results of available experimental data of ERCOFTAC.

Key words: axial turbine, endwall flow, secondary flow, enthalpy loss

1. Introduction

Endwall flows in turbine blade-to-blade passages are flows in endwall boundary layers and secondary flows. The secondary flows originate from specifically developing endwall boundary layers and are associated with the presence of longitudinal vortices with a dominant streamwise component of the vorticity. They are driven by transverse static pressure gradients and mass forces acting on fluid elements in curvilinear motion through the blade-to-blade passage. The secondary flows also modify the shape of endwall boundary layers from which they originate. Understanding the complex development of endwall flows is a part of understanding turbomachinery flows.

The problem of endwall flows, especially secondary flows, is discussed in the literature. There are a number of secondary flow models documenting the progress in our understanding of the secondary flows over the years. Some of these models will briefly be presented in Section 2. First, the secondary

flows in cascades without a tip clearance and relative motion of the blade tips and endwall will be considered. Also, the formation of secondary flows in tip clearance cascades will be discussed.

Endwall flows are also an important source of losses in turbines, especially in cascades with short-height blading and high flow turning. Due to the complex nature of endwall boundary layer flows and secondary flows, the evaluation of endwall losses is not an easy task. New formulas and methods are needed to calculate endwall losses. It is also expected that CFD methods can provide a powerful tool for the evaluation of endwall flows and losses in turbines.

2. Formation of endwall flows

The picture of endwall flows in turbine blade-to-blade passages is extremely complex, dominated by the presence of secondary flows. A few landmark models explaining the development of secondary flows are illustrated in Fig. 1. The main type of secondary flow is the induced recirculating flow, which leads to the formation of a passage vortex. The source of the induced recirculating flow is the cross flow in the endwall boundary layer that forms as a result of force equilibrium in curvilinear motion. The momentum equation in the cross-stream direction can be written in the form

$$\frac{\rho v^2}{R} = \frac{\partial p}{\partial n} \tag{2.1}$$

where v denotes the velocity, p is the pressure, ρ – density, R – streamline curvature radius, n – normal coordinate. With a decrease of the velocity in the boundary layer, a reduction of the streamline curvature radius in the boundary layer flow is required in order to balance the pitchwise pressure gradient formed in the channel. As a consequence, the boundary layer flow is turned more than the main flow in the blade-to-blade channel, leading to a crossflow from the pressure to suction surface in the endwall boundary layer. A compensating return flow must then occur at a certain distance from the endwall, giving rise to the recirculating flow described by e.g. Hawthorne (1951), Puzyrewski (1963), which can be seen in Fig. 1a. From this recirculating flow, a passage vortex is formed. Downstream in the blade-to-blade passage, due to the pressure-to-suction side pressure difference, the passage vortex locates near the blade suction surface. As a result of the recirculating flow in the

(a)

trailing vortex

passage vortex

(b)

passage vortex

counter vortex

endwall cross flow

(c)

suction side leg horse-shoe vortex

inlet boundary layer

passage vortex

suction side leg horse-shoe vortex

pressure side leg horse-shoe vortex (becomes passage vortex)

(d)

1. pressure side horse-shoe vortex
2. suction side horse-shoe vortex

separation lines

3. passage vortex
4. suction side corner vortices
5. pressure side corner vortex
6. pressure side/leading edge corner vortex
7. suction side/leading edge corner vortex
8. endwall cross flow

(e)

pressure side leg horse-shoe vortex

suction side leg horse-shoe vortex

corner vortex

passage vortex

corner vortex

saddle point

dividing stream surface

(f)

A-A B-B C-C

V_{wip}

V_{pc} V_{sh} C V_p

V_{ph} B V_{sc}

V_{plc} B C

V_{sh} V_{slc}

V_{sh}, V_{ph} - suction and pressure side horse-shoe vortex
V_p - passage vortex
V_{wip} - wall vortex induced by passage vortex

V_{slc}, V_{plc} - suction and pressure side leading edge corner vortex
V_{sc}, V_{pc} - suction and pressure side corner vortex

Fig. 1. Secondary flow models in turbine cascades: (a) – model of Hawthorne (1955), (b) – model of Langston (1980), (c) – model of Sharma and Butler (1987), (d) – model of Goldstein and Spores (1988), (e) – model of Doerffer and Amecke (1994), (f) – model of Wang *et al.* (1997)

neighbouring blade-to-blade passages, a vortex layer is formed at the trailing edge, which is quickly rolled-up downstream into a shed trailing edge vortex.

Another element of secondary flows is a horse-shoe vortex. The process of formation of the horse-shoe vortex upstream of the leading edge and its downstream transport was explained by Langston *et al.* (1980), Marchal and Sieverding (1977), Hodson and Dominy (1987), Eckerle and Langston (1987). The models of this process presented in these papers differ from one another in details only. The model illustrated in Fig. 2 comes from the paper by Marchal and Sieverding (1977). The boundary layer fluid upstream of the leading edge is decelerated by the adverse pressure gradient and separates at a saddle point s_1. The boundary layer fluid elements form a reverse recirculating flow just before the leading edge. This reverse flow separates at another saddle point s_2. The upstream boundary layer rolled-up in the recirculating zone flows past the leading edge and is transported downstream in two legs – pressure-side and suction-side leg of the horse-shoe vortex. The suction-side leg of the horse-shoe vortex moves near the suction surface of the blade. The pressure-side leg subject to the pressure gradient towards the suction surface moves across the blade-to-blade passage towards this surface. The legs of the horse-shoe vortex move along the lift-off lines that are lines of the saddle points as illustrated in Fig. 2. The location of the horse-shoe vortex lift-off lines, especially that of the
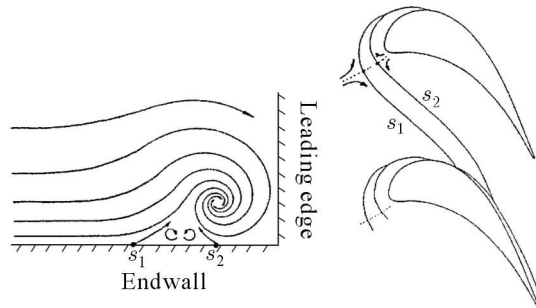
Fig. 2. Separation of the endwall boundary layer upstream of the blade leading edge and formation of the horse-shoe vortex; s_1, s_2 – saddle points, Marchal and Sieverding (1977)

pressure-side leg depends on the load of the front part of the blade. For the case of front-loaded profiles with high flow turning in the front part of the blade-to-blade passage, the lift-off line of the horse-shoe vortex pressure-side leg reaches earlier the vicinity of the suction surface than for the case of the aft-loaded profiles. All main forms of secondary flows meet at the suction surface of the blade. The model that explains the transport of the horse-shoe vortex, where

the pressure-side leg of the horse-shoe vortex together with the endwall cross flow form the main recirculating flow and the resulting passage vortex, whereas the suction-side leg of the horse-shoe vortex stays apart counter-rotating with respect to the passage vortex, comes from the work of Langston (1980) shown in Fig. 1b.

In the model of Sharma and Butler (1987) (Fig. 1c), the suction-side leg of the horse-shoe vortex is wrapped around the passage vortex, whereas in the model of Goldstein and Spores (1988) (Fig. 1d), the suction-side leg locates above the passage vortex and moves together with it. The picture looks similar in the model of Doerffer and Amecke (1994) (Fig. 1e), with a dividing stream surface between the passage vortex and the suction-side leg of the horse-shoe vortex. In point of the suction-side leg of the horse-shoe vortex, Wang *et al.* (1997) (Fig. 1f) return to the concept of Sharma and Butler (1987) – this leg of the horse-shoe vortex remains wrapped around the passage vortex. In addition to that, both legs of the horse-shoe vortex are formed not from a single vortical structure, but from a pair of alternatelly dissipating vortices.

At the trailing edge, the secondary kinetic energy of the suction-side leg of the horse-shoe vortex can be entirely dissipated as a result of shear interaction with the stronger passage vortex, Moore and Smith (1984), also Sieverding (1985). Thus, subregions of the sense of rotation opposite to that of the passage vortex may not be observed at the trailing edge section. Most papers also suggest that there will be no distinction within the passage vortex as to which part of it is due to the main recirculating flow or due to the pressure-side leg of the horse-shoe vortex. The investigations of Doerffer and Amecke (1994) indicate that the pressure-side leg of the horse-shoe vortex can be located in the core of the passage vortex. Results of the above investigations (all papers cited so far in this paper are experimental works) are also confirmed by results of visualisation of RANS-based numerical calculations of the subsonic linear Durham cascade (Gregory-Smith, 1993-2002) made by Doerffer *et al.* (2001). The visualisation was performed by means of streaklines originating from the regions of formation of various types of secondary flows and passing through the loss centres at the cascade exit section downstream of the trailing edge. It follows from this visualisation that the pressure-side leg of the horse-shoe vortex of the sense of rotation the same as that of the passage vortex concentrates inside the passage vortex region. The fluid elements coming from the suction-side leg of the horse-shoe vortex are distributed at the borders of the passage vortex, losing their rotation (originally opposite to that of the passage vortex) as a result of interaction with it. The mutual location and interaction of the passage vortex, pressure-side leg and suction-side leg of the

horse-shoe vortex are main elements differentiating the presented secondary flow models. On the one hand, the differences between the models reflect the progress in understanding of the endwall flows in the course of time. On the other hand, they suggest that depending on the cascade geometry and flow thermodynamics, the picture of secondary flows may be not uniform but subject to change, especially in point of mutual relations between the intensities of particular secondary flow structures.

The models of Goldstein and Spores (1988), Doerffer and Amecke (1994), Wang *et al.* (1997) also illustrate the presence of a number of tertiary vortex structures, including corner vortices. They are shear-driven secondary flows or structures formed as a result of separation of the main secondary flows in the corners between the endwall and pressure or suction side of the blade. More corner vortices, called the leading edge corner vortices, appear in the endwall/pressure or suction side corners at the leading edge. The model of Wang *et al.* (1997) features also a wall vortex induced above the passage vortex at the suction surface. This vortex appears at a location, which in the earlier models was reserved for the suction-side leg of the horse-shoe vortex (Goldstein and Spores, 1988; Doerffer and Amecke, 1994). It should be noted that real vortex structures have the rotating intensity much lower than that presented in Fig. 1, intentionally augmented for the sake of clarity.

The vorticity contours in the cascade exit section typically exhibit two strong peaks of the opposite signs, that is two counter-rotating vortex structures located close to each other at a some distance from the endwall. These vortex structures can be identified as the passage vortex and trailing shed vortex, Hawthorne (1951), Gregory-Smith and Cleak (1992). The trailing shed vortex originates from the vortex layer that is formed at the trailing edge due to the suction-to-pressure side velocity difference. Especially important is here the fact that the suction side velocity in the endwall region is affected by formation of the passage vortex. The vortex layer shed into the flow domain downstream of the trailing edge is quickly rolled up and assumes the sense of rotation opposite to that of the passage vortex. There is strong shear between the passage vortex and shed trailing edge vortex.

The centres of secondary vortices are regions of a high turbulence level. The turbulence level at the exit section of the Durham cascade in the passage vortex and trailing shed vortex measured by Gregory-Smith and Cleak (1992) was estimated at 35% with respect to the inlet velocity, yielding 16-17% with respect to the local downstream velocity. The turbulence level in the suction-side corner vortex is nearly as high as above. The increase of turbulent fluctuations in the region of secondary vortices can be attributed to

the process of deformation of the endwall boundary layer under conditions of high streamline curvature and acceleration of the main flow in the cascade. On the other hand, these vortex flows wash away the endwall boundary layer towards the suction surface and give rise to relaminarisation of the downstream endwall boundary layer. The newly formed endwall boundary layer becomes thin. It is gradually increasing in thickness but is constantly washed away. As a result, the endwall boundary layer has a highly three-dimensional character. Measurements of pressure pulsations in the endwall boundary layer made by Harrison (1989) and reproduced in this paper in Fig. 3 show that this boundary layer is in the major part laminar (downstream of the horse shoe vortex lift-off lines) or intermittent, and becomes turbulent only in the rear part of the blade-to-blade passage at the suction surface. For a more detailed description of formation of secondary vortices and flows in endwall regions the reader is requested to refer to the work by Gregory-Smith (1997).
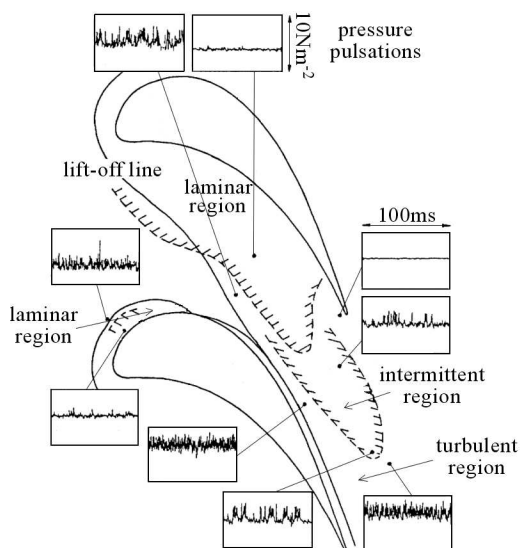
Fig. 3. Division of the endwall boundary layer into the regions of laminar, intermittent and turbulent flow, Harrison (1989)

Let us also consider the case of a cascade with a clearance. A schematic development of passage vortices and a tip leakage vortex in this case is depicted in Fig. 4 after Sjolander (1997). The presence of the tip gap over the blade usually eliminates the stagnation at the endwall, which typically occurs in the corner between the endwall and blade leading edge in the no-tip-gap configuration. Therefore, a horse-shoe vortex does not feature at the tip endwall unless the tip gap is very small. The flow at the tip endwall approaching
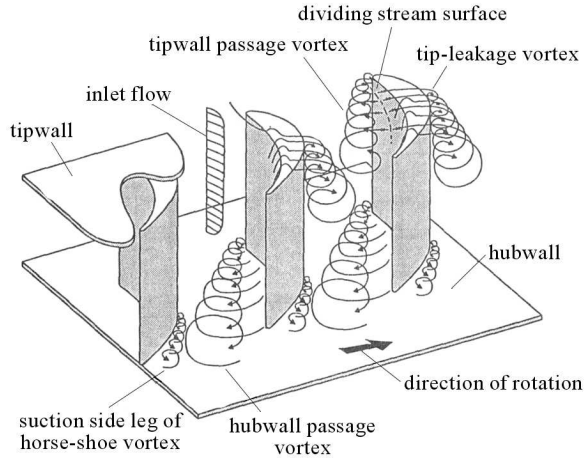
Fig. 4. Tip leakage and passage vortices at the tip endwall with a clearance,
Sjolander (1997)

the tip region above the leading edge of the blade is divided into two streams aiming towards low pressure regions at the suction surfaces of the neighbouring blades – a main stream of the tip leakage flow going through the tip gap over the blade and a stream of cross-flow going across the blade-to-blade passage. The tip leakage flow leaving the tip gap separates from the endwall under conditions of adverse pressure gradient and forms a tip leakage vortex. The cross-flow blocked by the development of the tip leakage vortex also separates from the endwall and rolls up into a passage vortex. The stream dividing line between the tip leakage and cross-flow lies at the pressure side of the blade tip. The tip leakage and passage vortices are characterised by the opposite sense of rotation. Usually, a dominant structure is the tip leakage vortex. The relations between the circulation and size of the two structures depend on many factors such as the tip gap size and flow turning angle.

3. Evolution of vorticity from the endwall boundary layer

The principal mathematical description of secondary flows draws on the spatial evolution of the vorticity vector in the cascade. This description enables better understanding of the phenomena associated with the secondary flows.

At the inlet to the cascade in a non-skewed endwall boundary layer, the vorticity can be assumed to have a direction normal to the main stream ve-

locity. During the flow through the cascade, the shear flow is turned, which gives rise to the production of longitudinal (streamwise) vorticity, whereas the normal component of the vorticity is also changed. The starting point to describe the evolution of the vorticity vector is the vorticity transport equation, which can be obtained from the momentum equation subject to the curl operator, e.g. Sherman (1990). The vorticity transport equation for a steady flow of a viscous compressible gas can be written as below (with the effect of mass forces neglected)

$$(\boldsymbol{u} \cdot \nabla)\boldsymbol{\omega} = (\boldsymbol{\omega} \cdot \nabla)\boldsymbol{u} - \boldsymbol{\omega}(\nabla \cdot \boldsymbol{u}) - \nabla \times \left(\frac{\nabla p}{\rho}\right) + \nabla \times \left(\frac{\nabla \cdot \boldsymbol{\tau}}{\rho}\right) \qquad (3.1)$$

where $\boldsymbol{u}$ is the velocity vector, $\boldsymbol{\omega}$ – vorticity vector, p – pressure, ρ – density, $\boldsymbol{\tau}$ – viscous stress tensor. Besides the left-hand-side convective term, the first right-hand-side term represents the vorticity production due to the velocity gradient (stretching and curving of vortex lines), second term – describes the vorticity production in a compressible flow (reduction in an expanding flow, increase in a compression region), third term – accounts for the baroclinic effect (in the field of spatial changes of pressure and density), fourth term – due to interaction of viscous forces in a compressible flow.

Lakshminarayana and Horlock (1973) presented a solution to this equation, which is of interest in turbomachinery applications. They assumed a coordinate system $(\boldsymbol{s}, \boldsymbol{n}, \boldsymbol{b})$, where $\boldsymbol{s}$ is the unit vector tangent to the streamline $\boldsymbol{u} = \boldsymbol{s}q$ (q – velocity magnitude), $\boldsymbol{n}$ is the unit normal vector directed towards the streamline curvature centre $\boldsymbol{n}/R = \boldsymbol{s} \cdot \nabla \boldsymbol{s}$ (R – streamline curvature radius), whereas $\boldsymbol{b}$ is the unit binormal vector $\boldsymbol{b} = \boldsymbol{s} \times \boldsymbol{n}$ so that $(\boldsymbol{s}, \boldsymbol{n}, \boldsymbol{b})$ is a right-handed set of vectors. The differential coefficients of the unit vectors of the system fulfil the following relations

$$\begin{aligned}
\frac{\partial \boldsymbol{s}}{\partial s} &= \frac{\boldsymbol{n}}{R} & \frac{\partial \boldsymbol{s}}{\partial n} &= \frac{\boldsymbol{n}}{a_n}\frac{\partial a_n}{\partial s} & \frac{\partial \boldsymbol{s}}{\partial b} &= \frac{\boldsymbol{b}}{a_b}\frac{\partial a_b}{\partial s} \\
\frac{\partial \boldsymbol{n}}{\partial s} &= \frac{\boldsymbol{b}}{\tau} - \frac{\boldsymbol{s}}{R} & \frac{\partial \boldsymbol{b}}{\partial s} &= -\frac{\boldsymbol{n}}{\tau}
\end{aligned} \qquad (3.2)$$

where τ is the radius of torsion of the streamline, a_n – distance in the $\boldsymbol{n}$ direction between neighbouring streamlines, a_b – distance in the $\boldsymbol{b}$ direction between neighbouring streamlines.

In the assumed coordinate system, changes of the pressure distribution in an inviscid flow are

$$\frac{\partial p}{\partial s} = -\frac{1}{2}\rho\frac{\partial q^2}{\partial s} \qquad \frac{\partial p}{\partial n} = -\frac{\rho q^2}{R} \qquad \frac{\partial p}{\partial b} = 0 \qquad (3.3)$$

Changes of the streamwise and normal component of the vorticity vector in the cascade, ω_s, ω_n, where $\boldsymbol{\omega} = \boldsymbol{s}\omega_s + \boldsymbol{n}\omega_n + \boldsymbol{b}\omega_b$, derived in Lakshminarayana and Horlock (1973) can be rewritten in the form

$$\rho q \frac{\partial}{\partial s}\left(\frac{\omega_s}{\rho q}\right) = \frac{2\omega_n}{R} - \frac{1}{q\rho^2}\left(\frac{\partial p}{\partial n}\frac{\partial \rho}{\partial b} - \frac{\partial \rho}{\partial n}\frac{\partial p}{\partial b}\right) + [\text{terms with viscosity}]$$

$$\frac{1}{q}\frac{\partial}{\partial s}(\omega_n q) = \frac{\omega_b}{\tau} - \frac{\omega_n}{a_b}\frac{\partial a_b}{\partial s} + \frac{1}{q\rho^2}\left(\frac{\partial p}{\partial s}\frac{\partial \rho}{\partial b} - \frac{\partial \rho}{\partial s}\frac{\partial p}{\partial b}\right) + [\text{terms with viscosity}]$$

(3.4)

In practical applications, Eq. $(3.4)_1$ for the streamwise vorticity seems to be of the main significance. Equation $(3.4)_2$ for the normal vorticity is not that widely used. Values of the normal vorticity can be found in an alternative way.

The above expressions do not expose terms connected with interaction of viscous forces, which in general have a very complex form. Although fluid elements that make up the passage vortex originate from endwall boundary layers, the dynamics of secondary flows within the blade-to-blade passage is often regarded in terms of interaction of the pressure and inertia forces, neglecting the viscous forces. The interaction of viscous forces is then limited to the formation of the inlet boundary layer and destruction of secondary vortex structures in the process of their mixing with the main flow downstream of the blade trailing edges. Lakshminarayana and Horlock (1973), also Horlock and Lakshminarayana (1973) obtained detailed solutions to Eqs. (3.4) for a number of model flow cases, including an inviscid constant-density flow, inviscid incompressible stratified flow (with constant density along streamlines), inviscid compressible flow of a barotropic fluid or perfect gas, viscous incompressible flow as well as inviscid incompressible flow in the rotating coordinate system.

In the most simple case of an inviscid incompressible flow with $\rho = \text{const}$, Eq. $(3.4)_1$ yields

$$\rho q \frac{\partial}{\partial s}\left(\frac{\omega_s}{\rho q}\right) = \frac{2\omega_n}{R}$$

(3.5)

Equation (3.5) indicates the effect of normal vorticity and streamline curvature on the process of generation of streamwise vorticity. Making use of an approximate assumption that the normal vorticity and velocity magnitude remain unchanged along the streamlines and integrating by substitution $d\alpha = ds/R$, yields the following equation (Squire and Winter, 1951)

$$\omega_s - \omega_{s0} = 2\omega_{n0}(\alpha - \alpha_0)$$

(3.6)

where ω_s is the current streamwise vorticity, ω_{s0} and ω_{n0} are the streamwise and normal vorticities at the inlet to the cascade (with $\omega_{s0} = 0$ for non-

skewed boundary layers), whereas the difference $\alpha - \alpha_0$ denotes the current flow turning in the cascade.

In a steady inviscid flow, streamlines and vorticity lines lie on surfaces of constant total pressure (Bernoulli surfaces), and the normal vorticity can be obtained from scalar multiplication of the Gromeko-Lamb equation by the unit binormal vector

$$\boldsymbol{b} \cdot (\boldsymbol{u} \times \boldsymbol{\omega}) = \boldsymbol{b} \cdot \frac{1}{\rho} \nabla \left(p + \frac{q^2}{2} \right) \;\; \Rightarrow \;\; \omega_n q = \frac{1}{\rho} \frac{\partial p^*}{\partial b} = \left| \frac{\nabla p^*}{\rho} \right| \cos \phi \qquad (3.7)$$

which turns Eq. (3.5) into the form (Hawthorne, 1955)

$$\rho q \frac{\partial}{\partial s} \left(\frac{\omega_s}{\rho q} \right) = \frac{2}{R \rho q} \frac{\partial p^*}{\partial b} \qquad \text{or} \qquad \left(\frac{\omega_s}{\rho q} \right)_2 - \left(\frac{\omega_s}{\rho q} \right)_1 = \int\limits_1^2 \frac{2}{R \rho q^2} \left| \frac{\nabla p^*}{\rho} \right| \cos \phi \, ds \tag{3.8}$$

where p^* is the total pressure, ϕ denotes the angle between the binormal versor and the normal to the Bernoulli surface (or direction of ∇p^*). Equation (3.7) exhibits a relationship between the streamwise vorticity and total pressure loss in the binormal direction. Equations (3.5) and (3.8) also remain valid for the case of an inviscid compressible flow of a barotropic fluid ($\rho = f(p)$ – which follows from the fact that in the assumed coordinate system $\partial p / \partial b = 0$, from which $\partial \rho / \partial b = 0$) and for the case of homoentropic flow of a perfect gas ($p / \rho^\kappa = \text{const}$). As shown in Shermann (1990), for the case of flow of a perfect gas with entropy gradients Eq. (3.8) reads as

$$\rho q \frac{\partial}{\partial s} \left(\frac{\omega_s}{\rho q} \right) = \frac{2}{R \rho^* q} \frac{\partial p^*}{\partial b} \tag{3.9}$$

where ρ^* denotes the density calculated from the state equation using stagnation parameters.

Lakshminarayana and Horlock (1973) also explain the effect of rotation on the development of secondary flows. The equation for the evolution of the vorticity along streamlines can be presented in the form (with viscous terms neglected)

$$\rho q \frac{\partial}{\partial s} \left(\frac{\omega_s}{\rho q} \right) = \frac{2 \omega_n}{R} + \frac{2 s \cdot (\boldsymbol{\Omega} \times \boldsymbol{\omega})}{q} - \frac{1}{q \rho^2} \left(\frac{\partial p}{\partial n} \frac{\partial \rho}{\partial b} - \frac{\partial \rho}{\partial n} \frac{\partial p}{\partial b} \right) \tag{3.10}$$

In the above equation, the vorticity is written in the absolute reference frame, whereas the streamlines are assumed in the rotating frame, thus $\boldsymbol{s}$ is the streamwise unit vector in the relative frame, q – relative velocity magnitude; $\boldsymbol{\Omega}$ – vector of the angular velocity of the rotating reference system. The

rotating term disappears as long as the Bernoulli surfaces remain cylindrical, which can be assumed approxiomate for the case of axial turbines. Therefore, rotation of the blade-to-blade channels does not influence secondary flows in axial turbines. The situation looks different in radial (radial/axial) turbomachines. More information on the physical nature of evolution of the streamwise vorticity in the secondary flow region can be found in Gregory-Smith (1997).

Based on the known distribution of the streamwise vorticity in the exit section, the exit velocity of the induced flow and the secondary kinetic energy can be evaluated. Assuming that this energy is lost in the process of mixing with the main flow, one can estimate the level of mixing losses. The velocity induced at the trailing edge section can be numerically calculated from the Poisson equation for the stream function ψ

$$\Delta \psi = -\omega_{s1} \tag{3.11}$$

The components of the induced secondary velocity v_{r1}, v_{n1} are then found as

$$v_{r1} = -\frac{\partial \psi}{\partial n} \qquad v_{n1} = \frac{\partial \psi}{\partial r} \tag{3.12}$$

The mass-averaged mixing loss coefficient due to secondary flows can be written as

$$\xi_{sec} = \frac{hp \int\limits_0^1 \int\limits_0^1 \rho_1 v_1 (v_{r1}^2 + v_{n1}^2) \cos \alpha_1 \; dxdy}{hp \int\limits_0^1 \int\limits_0^1 \rho_1 v_1^3 \cos \alpha_1 \; dxdy} \tag{3.13}$$

4.   Endwall loss sources

Production of endwall losses is a complex problem. Among basic loss mechanisms in the endwall and secondary flow regions are (Sieverding, (1985); Gregory-Smith, 1997):

- formation of the inlet boundary layer upstream of the blade leading edge,
- formation of the boundary layer downstream of the horse-shoe vortex lift-off lines,
- shear effects along the horse-shoe vortex lift-off lines, separation lines and along dividing surfaces between the passage vortex, other vortices, main flow and blade surfaces, especially at the suction surface,

- dissipation of the passage vortex, trailing shed vortex, corner vortices and other vortex flows in the process of their mixing with the main flow (it can be assumed that the secondary kinetic energy of the relative motion in the exit section is lost during mixing).

The processes of mixing due to secondary flows are usually not accomplished in the blade row where they originate and are continued in the downstream blade-to-blade passages. Considerable non-uniformities in the distribution of magnitude and direction of the velocity at the inlet to the subsequent blade row may lead to local separations and upstream relocation of the laminar-turbulent transition at the blade in the secondary flow dominated region.

The most decisive for the level of endwall losses are the blade span-to-chord ratio, flow turning in the cascade and inlet boundary layer thickness, which is accounted for in all experiment-based loss correlations for turbine cascades, e.g. Craig and Cox (1971), Traupel (1977). In the correlation of Traupel, the endwall losses are reversely proportional to the span-to-chord ratio in the blade span range in which there is no interference between secondary flow vortices from the opposite endwalls. For short blades this corelation is more complex. The endwall losses increase with the increased flow turning and increased inlet boundary layer thickness.

5. Endwall loss diagram

Denton (1999) evaluated the loss coefficient in the profile boundary layer by integrating the entropy production along the boundary layer. For an isolated turbine cascade, the profile loss coefficient can be expressed in the form

$$\zeta = \frac{T\Delta s}{\frac{1}{2}V_{\delta,te}^2} = \frac{T\dot{S}}{\frac{1}{2}V_{\delta,te}^2 m} = \sum \frac{C}{p} \frac{2}{\cos\alpha_1} \int_0^1 C_D \left(\frac{V_\delta}{V_{\delta,te}}\right)^3 d\left(\frac{x}{C}\right) \qquad (5.1)$$

where the integration extends on both sides of the profile, T denotes temperature, Δs – entropy rise, $\dot{S}$ – entropy production in the boundary layer, V_δ is the velocity at the edge of the boundary layer, $V_{\delta,te}$ – this velocity at the trailing edge, C_D – dissipation coefficient for a turbulent boundary layer ($C_D = 0.002$ – Schlichting (1968)), p – cascade pitch, C – profile chord, α_1 – exit angle (measured from the normal to the cascade front). The above formula exhibits the importance of the cube from the surface velocity V_δ^3 (referred to the exit isentropic velocity), state of the boundary layer, pitch/chord ratio and exit angle in generation of profile boundary layer losses.

The methods of evaluation of boundary layer losses in the profile boundary layers may not in general apply to endwall boundary layers. However, Harrison (1989) and Denton (1999) indicate that the losses in a specifically evolving endwall boundary layer can roughly be evaluated in a similar way assuming the dissipation coefficient as for turbulent flow. Thus, the entropy production in the endwall boundary layer upstream of the leading edge $\dot{S}_-$ and downstream of the trailing edge $\dot{S}_+$ can be found as

$$\dot{S}_- = 2C_D p \Delta x_- \rho \frac{V_{\delta,le}^3}{T_{\delta,le}} \qquad\qquad \dot{S}_+ = 2C_D p \Delta x_+ \rho \frac{V_{\delta,te}^3}{T_{\delta,te}} \qquad (5.2)$$

where $V_{\delta,le}$, $T_{\delta,le}$, $V_{\delta,te}$, $T_{\delta,te}$ denote velocities and temperatures at the edge of the boundary layer; Δx_-, Δx_+ are lengths of the endwall boundary layers, that is the distances along the endwalls from a referential inlet section to the leading edge and from the trailing edge to the exit section. The factor 2 in Eq. (5.2) indicates that both endwalls are considered. Any change of radius for annular cascades is neglected assuming the same value of pitch for both endwalls. Assuming that the mass flow rate is equal to $m = V_x \rho p h$, where h denotes the channel height, V_x is the axial velocity $V_x = V_{\delta,le} \cos \alpha_0 = V_{\delta,te} \alpha_1$ (α_0, α_1 – inlet and exit angles), and making use of the entropy definition of the loss coefficient $\xi = T\dot{S}/[0.5V_{\delta,te}^2 m]$, the following relations for the loss coefficient upstream of the leading edge ξ_- and downstream of the trailing edge ξ_+ can be derived

$$\xi_- = 4C_D \frac{\Delta x_-}{h} \frac{\cos^2 \alpha_1}{\cos^3 \alpha_0} \qquad\qquad \xi_+ = 4C_D \frac{\Delta x_+}{h} \frac{1}{\cos \alpha_1} \qquad (5.3)$$

The contribution of the first term is negligible for a low inlet-to-outlet velocity ratio in an expanding cascade, whereas the second term can be important for an extended boundary layer region downstream of the trailing edge Δx_+. The loss coefficient remains inversely proportional to the channel height and also to the flow turning in the second term.

The loss coefficient in the blade-to-blade region, that is between the leading and trailing edge will now be evaluated. The entropy production in the endwall boundary layer within the blade-to-blade passage $\dot{S}_M$ can be found as a surface integral

$$\dot{S}_M = 2C_D C_a p \int_0^1 \int_0^1 \frac{\rho V_\delta^3}{T_\delta} \, d\left(\frac{x}{C_a}\right) d\left(\frac{y}{p}\right) \qquad (5.4)$$

where C_a is the axial chord ($C_a = C \cos \gamma$, where γ denotes the stagger angle of the profile). The integral appearing above can be evaluated assuming a

linear velocity profile across the pitch (that is between the suction and pressure surface $V_\delta = V_p + (V_s - V_p)y$, $y \in \langle 0, 1 \rangle$, where V_s, V_p are not functions of the coordinate y), and also assuming a model of a thin profile evenly loaded along the chord with a constant suction-to-pressure surface velocity difference (that is $V_s - V_p = 2\Delta V = \text{const}$, $V_s + V_p = 2\overline{V}$, $\overline{V} \cos \alpha = V_x$, where α is the current flow angle in the cascade changing between the inlet and outlet angles α_0, α_1). The whole calculation procedure was described by Lampart (2006) and will not be repeated here. The following formula for the loss coefficient ζ_M accounting for the endwall boundary layer within the blade-to-blade passage was derived there

$$\zeta_M = \frac{T\dot{S}_M}{\frac{1}{2}V_{\delta,te}^2 m} = \frac{4C_D^2 \alpha_1 \cos \gamma}{\alpha_1 - \tan \alpha_0} \frac{C}{h} \frac{4}{3} c_1 \tag{5.5}$$

This formula was obtained for the velocity ratio $\Delta V / V_x = \sqrt{c_1/3c_2}$ corresponding to the minimum value of loss coefficient in the profile boundary layer, which is equivalent to the optimum pitch/chord ratio, and also assuming that the function $\tan \alpha$ changes linearly with the chord between $\tan \alpha_0$ and $\tan \alpha_1$. The functions c_1 and c_2 are

$$c_1 = \frac{1}{4} \left(\frac{\tan \alpha_1}{\cos^3 \alpha_1} - \frac{\tan \alpha_0}{\cos^3 \alpha_0} + 3c_2 \right)$$

$$c_2 = \frac{1}{2} \left(\frac{\tan \alpha_1}{\cos \alpha_1} - \frac{\tan \alpha_0}{\cos \alpha_0} + \ln \frac{\tan \alpha_1 + \frac{1}{\cos \alpha_1}}{\tan \alpha_0 + \frac{1}{\cos \alpha_0}} \right) \tag{5.6}$$

With the surface velocity cubed in the loss formula as well as with the linear surface velocity profile across the pitch postulated, and additionally assuming that $V_p = 0$, it can be shown that the mean endwall boundary layer losses per unit area form only $1/4$ of the mean profile boundary layer losses. In fact, the surface pressure velocity can not be neglected and the endwall losses are larger than that.

The sum of the endwall loss coefficients expressed by Eqs. (5.3) and (5.5), that is $\xi_- + \xi_M + \xi_+$ is plotted in Fig. 5 as a function of cascade inlet and exit angles for the chord/span ratio $C/h = 1$, stagger angle $\gamma = 30°$ (which gives the axial chord/span ratio $C_a/h = 0.866$) and for a typical axial extention of the inlet and exit region $\Delta x_\pm = C/4$. The boundary layer losses clearly increase with the increased exit angle. For a combination of inlet and exit angles typical for subsonic stator cascades of impulse turbines (e.g. with PŁK profiles – see part II of the paper) $\alpha_0 = (-10°, +10°)$, $\alpha_1 = (75°, 80°)$, the

endwall boundary layer loss coefficient calculated from Eqs. (5.3) and (5.5) changes between 1.8-2.5%. As indicated by Denton (1993), 2/3 of the overall endwall loss falls on endwall boundary layers. The other part comes from mixing of the inlet boundary layer in the region of secondary flow formation, and from dissipation of the kinetic energy of secondary vortices, typically 1/4 of the overall endwall loss.

For a combination of the inlet and exit angles typical for rotor cascades of impulse turbines (e.g. with R2 profiles – also see part II) $\alpha_0 = (-70°, -60°)$, $\alpha_1 = (70°, 75°)$, the endwall boundary layer loss coefficient calculated from Eqs. (5.3) and (5.5) changes between 1.5-2.0%, which is less than for the considered stator cascade. This can be explained by the lower cascade exit angle and, consequently, lower velocities in impulse stage rotor throats. But the overall endwall losses are by no means lower. In this case, the losses due dissipation of secondary vortices considerably increase.
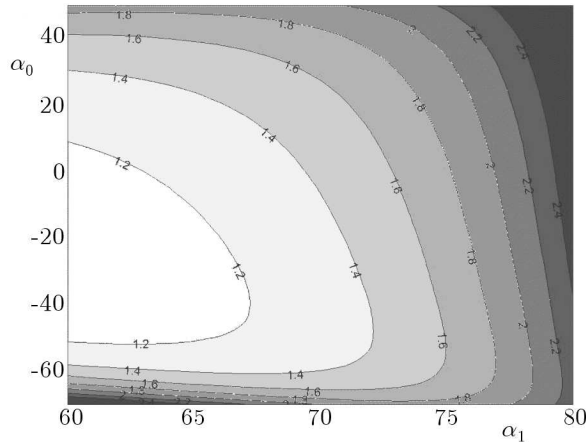
Fig. 5. Endwall boundary layer loss coefficient $\xi_- + \xi_+ + \xi_M$ for a given set of cascade inlet and exit angles calculated from Eqs. (5.3) and (5.5); $C/h = 1$, $C_a/h = 0.866$

The evaluation of losses due to mixing of secondary flows with the main stream using elementary methods is especially difficult since the secondary flow patterns have a very individual character depending on the cascade geometry and flow thermodynamics. These mixing losses were evaluated theoretically for an inviscid flow in the paper by Puzyrewski (1963). Based on the convection of vortex lines in a flow turning channel, the streamwise vorticity in the exit section was calculated there, from which the secondary kinetic energy was found. With the assumption that all this kinetic energy is dissipated, the

mixing loss coefficient was derived there as (after adaptation of the original formula to the denotations used in this paper)

$$\xi_{sec} = \frac{c_2}{\left(\alpha_1 + \frac{h}{C}\frac{C}{p}\right)^2} \frac{\sin^2(\alpha_1 - \alpha_0)}{(\cos\alpha_1 + \cos\alpha_0)^2} \frac{\cos^4\alpha_1}{\cos^4\alpha_0} \tag{5.7}$$

The above formula contains a constant c_2 whose value was obtained from correlation with experimental data for a few types of cascades, $c_2 = 0.159$. This formula explains large contribution of mixing losses due to secondary flows in cascades with front-loaded profiles having high negative inlet angles and high flow turning (typical in impulse stage rotor cascades, where $\alpha_0 < -60°$), whereas the mixing losses are relatively small for cascades with the zero inlet angle (as in stator cascades).

The increased possibilities of determination of mixing losses are connected with the development of 3D flow solvers.

6. Comparison of numerical results with ERCOFTAC data

A series of CFD computations of a 3D turbine cascade of Durham (Gregory-Smith, 1993-2002) were made with the help of 3D RANS solvers FlowER (finite volume method, upwind differencing, thrid-order ENO scheme, Baldwin-Lomax or Menter $k - \omega$ SST turbulence model, see Yershov and Rusanov (1997), Yershov *et al.* (1998)) and Fluent (finite volume method, second-order upwind, Reynolds Stress Model – having basic features of the Launder-Reece-Rodi model, see Fluent Inc. (2000)). The calculations converging to a steady-state were made in a one blade-to-blade passage of the rotor cascade on H or O-H type grids refined near the blade walls and endwalls ($y^+ = $ 1-2), leading and trailing edges of the blades. Typically, there were 12-16 grid cells in each boundary layer. The number of cells in one blade row reached 500 000 for H-type grids (92 axially, 76 radially, 72 pitchwise) and 1 000 000 for O-H grids.

Regions of accumulation of secondary flow losses are located at a some distance from the endwalls, Hodson and Dominy (1987), Gregory-Smith and Cleak (1992). The area distribution of total pressure downstream of the trailing edge in a Durham linear cascade (pitch/chord – 0.85, span/chord – 1.79, inlet angle $43°$, exit angle $-69°$) shown in Fig. 6 exhibits a strong loss centre containing two peaks due to the passage vortex and trailing shed vortex. Another loss centre is placed near the endwall in the region of the suction

side corner vortex. The total pressure peaks coincide with places characterised by the highest viscous stresses and are located near the places of maximum vorticity. The picture of secondary flows evolves downstream as a result of dissipative processes. In other cascades, depending on the distance from the trailing edge, the area distribution of total pressure in the exit section features only one peak in the secondary flow loss centre due to the passage vortex, see Langston *et al.* (1977), Yamamoto (1987).
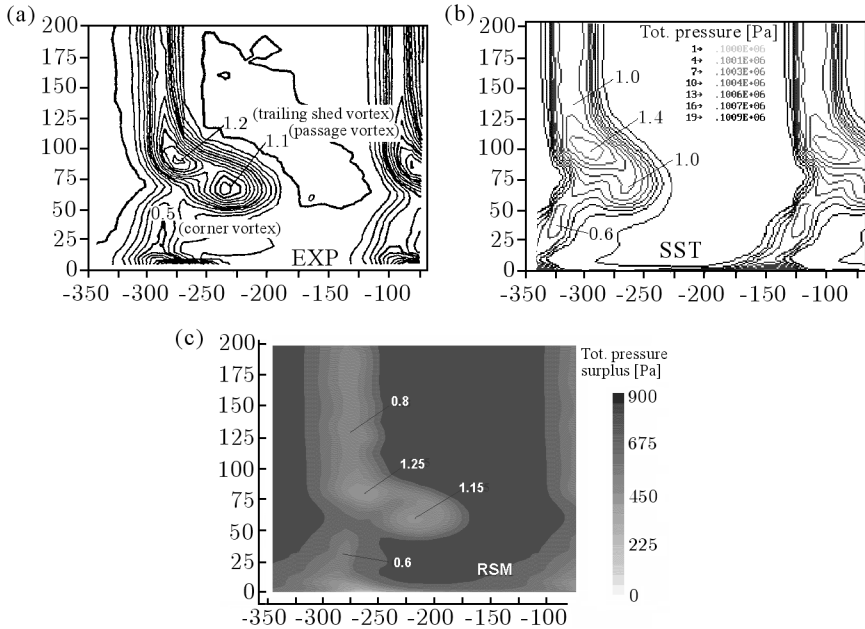
Fig. 6. Durham cascade – total pressure contours at the slot 10 (28% axial chord downstream of the trailing edge); (a) experimental (Gregory-Smith, 1993-2002), (b) computed by FlowER with $k - \omega$ SST, (c) computed by Fluent with RSM-LRR

The pitch-averaged spanwise distribution of the total pressure coefficient (referred to the inlet dynamic head) in the exit section of the Durham cascade illustrated in Fig. 6 shows a maximum at 20% of the blade span from the endwall. The secondary flows give rise to non-uniformities in the velocity field. In the secondary flow dominated region, the flow turning angle is decreased on the mid-span side of the secondary flow vortices, whereas on the endwall side it is increased. This flow underturning and overturning can also be observed in Fig. 7.

The comparison of experimental and computational results for the Durham cascade presented in Figs. 6 and 7 can be considered a validation of the computational methods used in this paper. The turbulent viscosity models
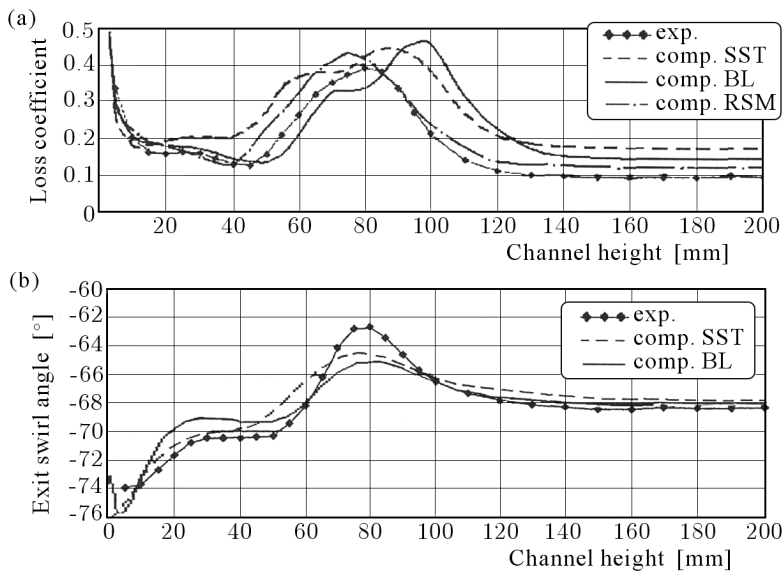
Fig. 7. Durham cascade – spanwise distribution of the loss coefficient (a) and exit swirl angle (b) at the slot 10 (28% axial chord downstream of the trailing edge); experimental (Gregory-Smith, 1993-2002), computed by FlowER with Baldwin-Lomax or Menter $k - \omega$ SST and computed by Fluent with RSM-LRR

seem to be able to qualitatively predict basic features of the secondary flows. However, they overpredict the level of losses in the wake and in the secondary flow region. Quantitative predictions are improved with the Reynolds stress model, but they are connected with a significant increase of computational costs.

7. Conclusions

The formation of endwall flows and evolution of vorticity from the endwall boundary layers was explained in the paper. Several models of secondary flows in turbine cascades were presented. An analytical expression was derived to approximately describe the level of losses in the endwall boundary layers by integrating the entropy increase in the endwall boundary layer and assuming a model of a thin profile evenly loaded allong the chord. The endwall losses were also calculated with the help of CFD in a 3D planar cascade of Durham and compared with the results of available experimental data of ERCOFTAC. The

calculations based on turbulent viscosity models are capable of capturing basic 3D flow effects in cascade flows. However, they overpredict the level of losses in the wake and in the secondary flow region. The quantitative predictions are improved with the Reynolds stress model, but they are connected with a significant increase of computational costs.

References

1. CRAIG H.R.M., COX H.J.A., 1971, Performance estimation of axial flow turbines, *Proc. Inst. Mech. Eng.*, **185**, 32/71, 407-424

2. DENTON J.D., 1993, Loss mechanisms in turbomachines, *Trans. ASME J. Turbomachinery*, **115**, 621-656

3. DENTON J.D., 1999, Loss mechanisms in turbomachines, Part I – Entropy creation in fluid flows, Part II – Loss generation in turbomachines, *VKI LS 1999-02*

4. DOERFFER P., AMECKE J., 1994, Secondary flow control and stream-wise vortices formation, *ASME Paper 94-GT-376*

5. DOERFFER P., RACHWALSKI J., MAGAGNATO F., 2001, Numerical investigation of the secondary flow development in turbine cascade, *TASK Q.*, **5**, 2, 165-178

6. ECKERLE W.A., LANGSTON L.S., 1987, Horseshoe vortex formation around a cylinder, *Trans. ASME, J. Turbomachinery*, **109**, 278-286

7. Fluent/UNS/Rampant, 2000, *User's Guide*, Fluent Inc.

8. GOLDSTEIN R.J., SPORES R.A., 1988, Turbulent transport on the endwall in the region between adjacent turbine blades, *Trans. ASME, J. Heat Transfer*, **110**, 862-869

9. GREGORY-SMITH D.G., 1993-2002, Durham low-speed turbine cascade, Turbomachinery workshop test case No. 3, *Proc. ERCOFTAC Seminar and Workshop on Turbomachinery Flow Prediction*, **I-VIII**

10. GREGORY-SMITH D.G., 1997, Secondary and tip-clearance flows in axial turbines, *VKI LS 1997-01*

11. GREGORY-SMITH D.G., CLEAK J.G.E., 1992, Secondary flow measurements in a turbine cascade with high inlet turbulence, *Trans. ASME, J. Turbomachinery*, **114**, 173-183

12. HARRISON S., 1989, Secondary loss generation in a linear cascade of high turning turbine blades, *Trans. ASME, J. Turbomachinery*, **111**, 618-624

13. Hawthorne W.R., 1951, Secondary circulation in fluid flow, *Proc. Roy. Soc. Ser. A*, **206**, 374-387

14. Hawthorne W.R., 1955, Rotational flow through cascades, *Quart. J. Mech. Appl. Math.*, **8**, 3, 266-279

15. Hodson H.P., Dominy R.G., 1987, Three-dimensional flow in a low pressure turbine cascade at its design conditions, *Trans. ASME, J. Turbomachinery*, **109**, 278-286

16. Horlock J.H., Lakshminarayana B., 1973, Secondary flows: theory, experiment, and application in turbomachinery aerodynamics, *Ann. Rev. Fluid Mechanics*, **5**, 247-279

17. Lakshminarayana B., Horlock J.H., 1973, Generalised expressions for secondary vorticity using intrinsic co-ordinates, *J. Fluid Mech.*, **59**, Part 1, 97-115

18. Lampart P., 2006, CFD investigation of aerodynamics of turbine blading systems, *Zeszyty Naukowe IMP PAN*, **544/1503/2006** [in Polish]

19. Langston L.S., 1980, Crossflows in a turbine cascade passage, *Trans. ASME, J. Eng. Power*, **102**, 866-874

20. Langston L.S., Nice M.L., Hooper R.M., 1977, Three dimensional flow within a turbine cascade passage, *Trans. ASME, J. Eng. Power*, **99**, 21-28

21. Marchal Ph., Sieverding C.H., 1977, Secondary flows within turbomachinery bladings, *Proc. AGARD-CP-24 Secondary Flows in Turbomachines*, **11**

22. Moore J., Smith B.L., 1984, Flow in a turbine cascade: Part 2 – Measurements of flow trajectories by ethylene detection, *Trans. ASME, J. Eng. Gas Turbines and Power*, **106**, 409-414

23. Puzyrewski R., 1963, Convection of vortex lines in curved ducts as a means for calculation of endwall losses, *Trans. IFFM*, **17**, 63-108 [in Polish]

24. Schlichting H., 1968, *Boundary Layer Theory*, McGraw-Hill, New York

25. Sharma O.P., Butler T.L., 1987, Prediction of endwall losses and secondary flows in axial flow turbine cascades, *Trans. ASME J. Turbomachinery*, **109**, 229-236

26. Shermann F.S., 1990, *Viscous Flow*, McGraw-Hill, New York

27. Sieverding C.H., 1985, Recent progress in understanding of basic aspects of secondary flows in turbine blade passages, *Trans. ASME, J. Eng. Gas Turbines and Power*, **107**, 248-257

28. Sjolander S.A., 1997, Secondary and tip-clearance flows in axial turbines, *VKI LS 1997-01*

29. Squire H.B., Winter K.G., 1951, The secondary flow in a cascade of aerofoils in a non-uniform stream, *J. Aeronaut. Sci.*, **18**, 271-277

30. Traupel W., 1977, *Thermische Turbomaschinen, Band I*, Springer-Verlag, Berlin

31. Wang H.P, Olson S.J., Goldstein R.J., Eckert E.R.G., 1997, Flow visualisation of a linear turbine cascade of high performance turbine blades, *Trans. ASME J. Turbomachinery*, **119**, 1-8

32. Yamamoto A., 1987, Production and development of secondary flows and losses in two types of straight turbine cascades: Part 1 – A stator case, Part 2 – A rotor case, *Trans. ASME J. Turbomachinery*, **109**, 186-200

33. Yershov S., Rusanov A., 1997, The application package FlowER for the calculation of 3D viscous flows through multi-stage machinery, Certificate of registration of copyright, *Ukrainian State Agency of Copyright and Related Rights*, Kiev, February 19

34. Yershov S., Rusanov A., Gardzilewicz A., Lampart P., Świrydczuk J., 1998, Numerical simulation of viscous compressible flows in axial turbomachinery, *TASK Quart.*, **2**, 2, 319-347

Badanie przepływów i strat brzegowych w turbinach osiowych. Część I. Formowanie się przepływów w strefie brzegowej i strat brzegowych

Streszczenie

Przepływy brzegowe stanowią jedno z głównych źródeł strat w turbinach. W pracy w skrócie wyjaśniono proces formowania się przepływów brzegowych i ewolucję wirowości pochodzącej z brzegowych warstw przyściennych. Przedyskutowano wynikające stąd straty przepływu. Wyznaczono teoretycznie straty przepływu w brzegowej warstwie przyściennej poprzez całkowanie przyrostu entropii wzdłuż warstwy brzegowej i zakładając pewien model obciążenia profilu łopatkowego. Z pomocą programów komputerowych numerycznej mechaniki płynów wyznaczono także przepływ i straty brzegowe w prostej palisadzie turbinowej Durham i porównano otrzymane rezultaty z danymi eksperymentalnymi ERCOFTAC.